



A Global Two-scale Helicity Proxy from π -ambiguous Solar Magnetic Fields

Axel Brandenburg^{1,2,3,4}

¹ Nordita, KTH Royal Institute of Technology and Stockholm University, Roslagstullsbacken 23, SE-10691 Stockholm, Sweden; brandenb@nordita.org

² Department of Astronomy, AlbaNova University Center, Stockholm University, SE-10691 Stockholm, Sweden

³ JILA and Laboratory for Atmospheric and Space Physics, University of Colorado, Boulder, CO 80303, USA

⁴ McWilliams Center for Cosmology & Department of Physics, Carnegie Mellon University, Pittsburgh, PA 15213, USA

Received 2019 June 10; revised 2019 August 5; accepted 2019 August 26; published 2019 September 26

Abstract

If the α effect plays a role in the generation of the Sun’s magnetic field, the field should show evidence of magnetic helicity of opposite signs at large and small length scales. Measuring this faces two challenges: (i) in weak-field regions, horizontal field measurements are unreliable because of the π ambiguity, and (ii) one needs a truly global approach to computing helicity spectra in the case where one expects a sign reversal across the equator at all wavenumbers. Here we develop such a method using spin-2 spherical harmonics to decompose the linear polarization in terms of the parity-even and parity-odd E and B polarizations, respectively. Using simple one- and two-dimensional models, we show that the product of the spectral decompositions of E and B , taken at spherical harmonic degrees that are shifted by one, can act as a proxy of the global magnetic helicity with a sign that represents that in the northern hemisphere. We then apply this method to the analysis of solar synoptic vector magnetograms, from which we extract a pseudo-polarization corresponding to a “ π -ambiguated” magnetic field, i.e., a magnetic field vector that has no arrow. We find a negative sign of the global EB helicity proxy at spherical harmonic degrees of around 6. This could indicate a positive magnetic helicity at large length scales, but the spectrum fails to capture clear evidence of the well-known negative magnetic helicity at smaller scales. This method might also be applicable to stellar and Galactic polarization data.

Key words: dynamo – magnetic fields – polarization – techniques: polarimetric

1. Introduction

The magnetic field of the Sun and other late-type stars is known to have, on average, opposite signs of magnetic helicity in the northern and southern hemispheres (Seehafer 1990; Pevtsov et al. 1995). There is also the possibility of the field being bihelical (Blackman & Brandenburg 2003) with a sign change of the magnetic helicity at large length scales. To detect this in the Sun, one would need to measure *spectra* of magnetic helicity, but this is made complicated by the fact that the solar surface also displays a systematic north–south variation with opposite signs in the two hemispheres. To capture this correctly, a global approach must be adopted that takes the systematic north–south variation into account. This is done by utilizing what is known as a two-scale approach (Roberts & Soward 1975). Here, one scale is that of the large-scale hemispheric modulation, and the other is the scale of the turbulence, which in itself comprises an entire range of length scales. In that approach, one can compute a spectrum covering both north and south, while taking a systematic north–south variation into account as if both hemispheres looked just like the northern hemisphere (Brandenburg et al. 2017b, hereafter BPS).

The problem with the standard two-scale approach is that it is only a *semi-global* one. Technically, it is still Cartesian in that the solar surface magnetic field is represented in the Lambert cylindrical equal-area projection. In a proper global approach, by contrast, one would need to employ a spherical harmonics decomposition, but this must be done in such a way that the systematic north–south variation can still be taken into account.

In this paper, a simple heuristic modification to the usual spherical harmonics spectra is proposed. It is based on the idea that in the semi-global two-scale approach, the helicity

spectrum is computed as the product of the magnetic field and its vector potential at wavenumbers that are offset for the two fields by a small amount that corresponds to the wavenumber of the large-scale hemispheric modulation. Analogously, for spherical harmonics spectra, one should consider the product of the two terms at spherical harmonic degrees that are shifted by one. This idea is then adapted to analyzing also the parity-even and parity-odd contributions to the linear polarization (Kamionkowski et al. 1997; Seljak & Zaldarriaga 1997). The reason for using such a decomposition is that there are large uncertainties owing to the π ambiguity of the magnetic field in weak-field regions of the Sun. This ambiguity reflects the fact that polarization “vectors” have neither head nor tail.

Various disambiguation procedures are available (Sakurai et al. 1985; Georgoulis 2005; Hoeksema et al. 2014; Rudenko & Anfinogentov 2014), but they tend to fail in regions far away from sunspots, where the magnetic field is weak. To avoid any bias, the random disambiguation method is often employed (Liu et al. 2017). This is justified when the Stokes Q and U parameters are dominated by noise but, if this were indeed the case, it should not be possible to detect any systematic north–south dependence of the parity-odd EB correlation from weak-field regions. It is also clear that any magnetic helicity derived from a randomly disambiguated magnetic field may itself be random and would therefore be unreliable.

The proper way out of this problem of obtaining a qualitative measure of the Sun’s magnetic helicity from π -ambiguous magnetic fields is to work directly with the original linear polarization. This has already been attempted by determining the rotationally invariant parity-even and parity-odd contributions, or E and B polarizations, respectively, from the Stokes Q and U parameters (Brandenburg et al. 2019,

hereafter BBKMRPS). This decomposition yields a field that is parity even, i.e., statistically mirror symmetric, and another one that is parity odd, i.e., statistically mirror antisymmetric (Kamionkowski et al. 1997; Seljak & Zaldarriaga 1997). The relevant diagnostic quantity is usually the cross-correlation of the spectral representations of E and B (Kahniashvili & Ratra 2005; Kahniashvili et al. 2014; Bracco et al. 2019).

Attempts to analyze solar E and B polarizations have not yet produced a nonvanishing cross correlation (BBKMRPS). However, this could be caused by their method still being provisional in that only a semi-global approach was used to deal with the fact that the sign of the cross-correlation is systematically different in the northern and southern hemispheres. It was always clear that a proper analysis should involve a decomposition into spherical harmonics. More precisely, the linear polarization parameters Q and U must be decomposed into what is known as spin-2 spherical harmonics, which have the appropriate transformation properties for linear polarization (Kamionkowski et al. 1997; Seljak & Zaldarriaga 1997); see Durrer (2008) for a textbook on the subject. While this method is now routinely applied in cosmology using data from the *Planck* satellite (Planck Collaboration results XI 2018), it has not yet been adapted to the case where one expects there to be a global sign change of magnetic helicity about the equator. In that case, we employ the spherical harmonics decomposition of E and B , which yields $\tilde{E}_{\ell m}$ and $\tilde{B}_{\ell m}$, respectively. We then compute their product at spherical harmonic degrees that are shifted by one, i.e., we compute $\tilde{E}_{\ell m}\tilde{B}_{\ell+1 m}^*$. We also compute $\tilde{E}_{\ell m}\tilde{B}_{\ell-1 m}^*$, which we shall show to be a better proxy of the expected magnetic helicity spectrum than the former one.

The work of BBKMRPS suffered from another problem in that the publicly available polarization data were not cleaned and corrected to the same extent as those finally used to compute the Sun's magnetic field (Hughes et al. 2016). For example, the quality of the images varied across the solar disk. Furthermore, proper line fits to solar atmosphere models have not been performed. Therefore, there is a possibility of small shifts in frequency that could affect the resulting Q and U signals. In particular, the magnetic field can have different strengths at different geometrical depths, giving rise to more complicated spectral line profiles that are usually fully accounted for in the inversion pipelines (Hoeksema et al. 2014), but they were ignored in the more rudimentary analysis of BBKMRPS. A legitimate way out of this additional problem is to use the full solar magnetic field inversion along with its questionable disambiguated magnetic field and make it ambiguous again! We can do this by computing a synthetic (or pseudo) linear polarization from the horizontal magnetic field. Such work is already in progress (A. Prabhu 2019, in preparation), but it is still local and constrained to finite patches in one hemisphere, as was done in the works of BPS and Singh et al. (2018). Here, by contrast, we employ a novel analysis using spin-2 spherical harmonics to compute a global cross-correlation spectrum.

We begin by testing the global two-scale approach and its ability to extract a unique spectrum by using data from both hemispheres at the same time. In Section 2, we first construct simple axisymmetric fields to study the effects of a global sign change of the magnetic helicity. In Section 3, we consider nonaxisymmetric magnetic fields to verify the numerical approach. In Section 4, we use synoptic magnetograms from

Carrington rotations (CRs) 2161 to 2163, for which a semi-global helicity spectrum was previously determined (BPS). We discuss the relevance of our results for dynamo theory in Section 5 and conclude with the broader implications of the present work in Section 6.

2. An Axisymmetric Example

2.1. Representation of the Magnetic Field

It is useful to begin with a simple example that is similar in spirit to the one-dimensional example used in BPS (see their Figure 1), where the magnetic helicity density shows a sign change in the middle of the domain. For this purpose, we restrict ourselves to an axisymmetric magnetic field, which can be written in the form

$$\mathbf{b} = \nabla \times (a_\phi \hat{\phi}) + b_\phi \hat{\phi}, \quad (1)$$

where r and θ are radius and colatitude, $a_\phi(r, \theta)$ is the toroidal component of the magnetic vector potential, and $b_\phi(r, \theta)$ is the toroidal component of the magnetic field itself. The proper expansion of a_ϕ and b_ϕ is in terms of the associated Legendre polynomials $P_l^1(\cos\theta)$ as

$$a_\phi \hat{\phi} = \sum_{\ell=1}^{N_\ell} \tilde{a}_\ell(r) P_\ell^1(\cos\theta), \quad b_\phi \hat{\phi} = \sum_{\ell=1}^{N_\ell} \tilde{b}_\ell P_\ell^1(\cos\theta), \quad (2)$$

where N_ℓ determines the truncation level. The two horizontal magnetic field components on the surface of the sphere at $r = R$, say, are then given by

$$b_\theta(\theta) = -\frac{1}{R} \sum_{\ell=1}^{N_\ell} \frac{\partial}{\partial r}(r \tilde{a}_\ell) P_\ell^1(\cos\theta), \quad (3)$$

$$b_\phi(\theta) = \sum_{\ell=1}^{N_\ell} \tilde{b}_\ell P_\ell^1(\cos\theta). \quad (4)$$

Even if $\tilde{a}_\ell(r)$ were independent of r , the values of b_θ would be finite because of the r factor under the derivative. At the surface, however, it is more likely that $\tilde{a}_\ell(r)$ decays with r as a power law, for example like $r^{-(\ell+1)}$, as it would if the exterior magnetic field was a potential field (Krause & Rädler 1980). In such a case, b_ϕ would normally vanish, but this will not be assumed here, because then the magnetic field would have vanishing helicity. Specifically, we are interested in a field with globally antisymmetric magnetic helicity, so we assume that b_ϕ remains finite at $r = R$.

2.2. Opposite Helicities in the Two Hemispheres

In BPS, we constructed a magnetic field with globally antisymmetric helicity by having the two horizontal field components with a relative wavenumber shift that corresponds to the scale of the latitudinal variation of the magnetic helicity. This corresponds to the two components having an ℓ value that is different by one. In the present case, we choose $b_\ell = b_0$ and $a_\ell = -b_0 R / \ell$, with some general amplitude factor b_0 , so

$$b_\theta(\theta) = -b_0 P_\ell^1(\cos\theta), \quad b_\phi(\theta) = b_0 P_{\ell+1}^1(\cos\theta). \quad (5)$$

Analogously to BBKMRPS, we compute the complex linear polarization at $r = R$ as

$$p \equiv Q + iU = -\epsilon(b_\theta + i b_\phi)^2, \quad (6)$$

Table 1
First Few Spin-2 Spherical Harmonics

ℓ	m	${}_2Y_{\ell m}(\theta, \phi)$
2	0	$(3/4)\sqrt{5/6\pi} \sin^2 \theta$
2	± 1	$-(1/4)\sqrt{5/\pi} \sin \theta (1 \mp \cos \theta) e^{\pm i\phi}$
2	± 2	$(1/8)\sqrt{5/\pi} (1 \mp \cos \theta)^2 e^{\pm 2i\phi}$
3	0	$(1/4)\sqrt{105/2\pi} \sin^2 \theta \cos \theta$
4	0	$(15/4)\sqrt{9/10\pi} \sin^2 \theta [1 - (7/6)\sin^2 \theta]$
4	± 3	$(1/4)\sqrt{63/2\pi} \sin \theta (1 \mp \cos \theta) [(1 \mp \cos \theta)/2 - \sin^2 \theta] e^{\pm 3i\phi}$

where ϵ is the emissivity, which is here assumed to be constant. The minus sign in front of ϵ accounts for the fact that polarization is related to the electric field, which is at right angles to the magnetic field.

2.3. Spin-weighted Spherical Harmonics

Next, we decompose $p(\theta)$ into spin-weighted spherical harmonics (Kamionkowski et al. 1997; Seljak & Zaldarriaga 1997). The following expressions readily apply to the nonaxisymmetric case where the complex polarization also depends on longitude ϕ , i.e., $p = p(\theta, \phi)$. The spin-weighted spherical harmonics are computed as (Goldberg et al. 1967)

$${}_s Y_{\ell m}(\theta, \phi) = {}_s \mathcal{N}_{\ell m} {}_s \mathcal{P}_{\ell m}(\sin(\theta/2), \cos(\theta/2)) e^{im\phi}, \quad (7)$$

where

$${}_s \mathcal{N}_{\ell m} = (-1)^m \sqrt{\frac{2\ell + 1}{4\pi}} \frac{(\ell + m)!}{(\ell + s)!} \frac{(\ell - m)!}{(\ell - s)!} \quad (8)$$

is a normalization factor,

$${}_s \mathcal{P}_{\ell m}(x, y) = x^{2\ell} \sum_{r=0}^{\ell-s} {}_{rs} \mathcal{M}_{\ell m}(y/x)^{2r+s-m} \quad (9)$$

are polynomials of x and y/x , and

$${}_{rs} \mathcal{M}_{\ell m} = \binom{\ell - s}{r} \binom{\ell + s}{r + s - m} (-1)^{\ell - r - s} \quad (10)$$

is yet another normalization factor, where the binomials are defined to be zero when either of the arguments or their difference is nonpositive. In Table 1, we list a few selected spin-2 spherical harmonics.

The numerical application of Equation (9) can become problematic in the first (second) quadrant for $m > 0$ ($m < 0$) and $\theta \rightarrow 0$ ($\theta \rightarrow \pi$), because the sum has large terms of alternating sign. This is not the case in the correspondingly other quadrant. However, for the cases listed in Table 1, we observe that ${}_2Y_{\ell m}(\theta, \phi) = {}_2Y_{\ell -m}(\pi - \theta, \phi)$, although this relation is not generally true.

2.4. Spin-2 Spherical Harmonics Decomposition

We now compute the spin-2 spherical harmonics representation of $E + iB$ in terms of $Q + iU$ as (Kamionkowski et al. 1997; Seljak & Zaldarriaga 1997; Durrer 2008; Kamionkowski & Kovetz 2016)

$$\tilde{R}_{\ell m} = \int_{4\pi} (Q + iU) {}_2Y_{\ell m}^*(\theta, \phi) \sin \theta d\theta d\phi, \quad (11)$$

and define $\tilde{E}_{\ell m} = (\tilde{R}_{\ell m} + \tilde{R}_{\ell, -m}^*)/2$ as the parity-even part and $\tilde{B}_{\ell m} = (\tilde{R}_{\ell m} - \tilde{R}_{\ell, -m}^*)/2i$ as the parity-odd part in spectral space, where the asterisk means complex conjugation, and commas have been used to separate ℓ from $-m$. In the axisymmetric case, we have $m = 0$ and drop the index m . Furthermore, \tilde{E}_{ℓ} and \tilde{B}_{ℓ} are then real. It should also be noted that our coefficients $\tilde{E}_{\ell m}$ and $\tilde{B}_{\ell m}$ are sometimes defined with the opposite sign (see, e.g., Zaldarriaga & Seljak 1997). Here we follow the sign convention of the textbook by Durrer (2008).

The spatial dependencies of $E(\theta, \phi)$ and $B(\theta, \phi)$ are given by the real and imaginary parts of the inverse transform, R , i.e.,

$$E + iB \equiv R = \sum_{\ell=2}^{N_f} \sum_{m=-\ell}^{\ell} \tilde{R}_{\ell m} Y_{\ell m}(\theta, \phi). \quad (12)$$

It turns out that for a magnetic field given by Equation (5), finite values of \tilde{E}_{ℓ} are only obtained for even ℓ ($\ell \geq 2$), while finite values of \tilde{B}_{ℓ} are only obtained for odd ℓ ($\ell \geq 3$). In Figure 1, we show the θ dependence of the components of the two surface components of \mathbf{b} , as well as the fields (Q, U) and (E, B) for several values of ℓ .

In Figure 1, we also show a_{ϕ} , which is just $b_{\theta}R/\ell$, where the ℓ factor comes from the r derivative in Equation (3) and the fact that $\tilde{a}_{\ell}(r) \propto r^{-\ell+1}$. We choose $\tilde{b}_{\ell} = -\ell \tilde{a}_{\ell}/R = b_0$. In that case, positive contributions to the local magnetic helicity density, $h(\theta) = 2a_{\phi}b_{\phi}$ (Brandenburg et al. 2002), come from $\pi/2 \leq \theta \leq \pi$, i.e., from the southern hemisphere. Negative contributions come from the northern hemisphere. This corresponds to what is seen on the Sun for the small-scale field, i.e., the field with $k > 0.1 \text{ Mm}^{-1}$. We emphasize here that the corresponding scale, $2\pi/0.1 \text{ Mm}^{-1} \approx 60 \text{ Mm}$, is obviously not small by some standards, but it is small relative to the large-scale field of the Sun that manifests itself through the 11 yr cycle and the hemispheric antisymmetry of the mean toroidal field.

To distinguish the spherical harmonic degrees of the magnetic field from those of the E and B polarization, we denote the former with a prime as ℓ' . In order to have negative (positive) contributions to the local magnetic helicity density in the northern (southern) hemisphere, we now choose analogously to Equation (5),

$$\tilde{a}_{\ell} = -\delta_{\ell} \ell', \quad \tilde{b}_{\ell} = \delta_{\ell} \ell' + 1, \quad (13)$$

for selected values of ℓ' . Thus, for $\ell' = 1$, for example, we have $\tilde{a}_1 = -1$ and $\tilde{b}_2 = 1$ as the only two nonvanishing coefficients, so

$$b_{\theta} = -P_1^1(\cos \theta) = \sin \theta$$

$$\text{and } b_{\phi} = P_2^1(\cos \theta) = -3 \sin \theta \cos \theta.$$

In Tables 2 and 3, we list the two-scale polarization spectra

$$K_{\ell}^+ = \tilde{E}_{\ell} \tilde{B}_{\ell+1}^* \quad \text{and} \quad K_{\ell}^- = \tilde{E}_{\ell} \tilde{B}_{\ell-1}^*, \quad (14)$$

respectively, for different values of ℓ' . We note here again that, because $m = 0$, \tilde{E}_{ℓ} and $\tilde{B}_{\ell \pm 1}$ are real, so we can drop the asterisk. In all cases, the integral of $h(\theta)$ over both hemispheres vanishes. To get a sense of the strength of helicity, we therefore list in Tables 2 and 3 the rms value, h_{rms} . We see that h_{rms} increases only mildly with increasing values of ℓ' . By contrast, the extrema of $\tilde{E}_{\ell} \tilde{B}_{\ell+1}$ and $\tilde{E}_{\ell} \tilde{B}_{\ell-1}$ increase much faster with ℓ . This suggests that the ℓ -dependence of K_{ℓ}^- does not reflect the actual ℓ -dependence of magnetic helicity.

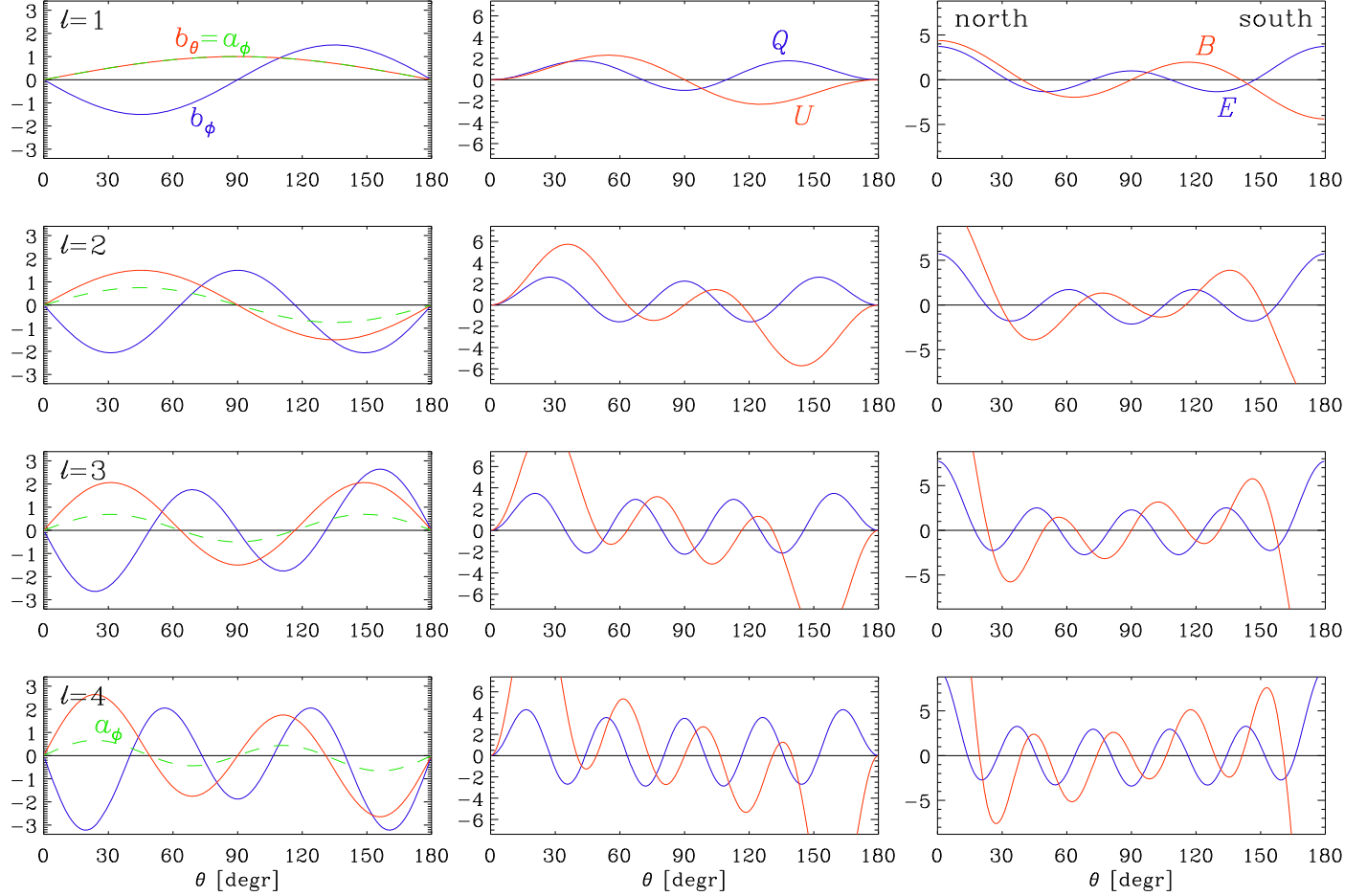


Figure 1. Latitudinal dependence of a_ϕ (dashed green), b_ϕ (blue), and b_θ (red) (left column), Q (blue) and U (red) (middle column), and E (blue) and B (red) (right column) for the one-dimensional model.

Table 2
Results for $\tilde{E}_\ell \tilde{B}_{\ell+1}$

ℓ'	ℓ						
	2	4	6	8	10	12	h_{rms}
1	4.3	0.0	0.0	0.0	0.0	0.0	1.50
2	6.5	-3.1	0.0	0.0	0.0	0.0	1.57
3	8.3	3.9	-13.6	0.0	0.0	0.0	1.69
4	10.1	5.3	2.1	-28.0	0.0	0.0	1.82
5	12.0	6.5	4.0	0.0	-46.4	0.0	1.95
6	13.9	7.5	5.0	2.9	-2.5	-65.7	1.95

Note. The maxima for each ℓ' are in bold.

Table 3
As Table 2, but for $\tilde{E}_\ell \tilde{B}_{\ell-1}$

ℓ'	ℓ						
	4	6	8	10	12	14	h_{rms}
1	22.6	0.0	0.0	0.0	0.0	0.0	1.50
2	-2.1	46.3	0.0	0.0	0.0	0.0	1.50
3	3.8	-8.4	77.9	0.0	0.0	0.0	1.69
4	5.7	1.9	-16.6	117.4	0.0	0.0	1.82
5	7.2	4.1	0.0	-26.6	165.0	0.0	1.95
6	8.6	5.4	2.8	-2.1	-38.6	220.5	2.08

Table 4
Similar to Tables 2 and 3, but Now Just for \tilde{B}_ℓ

ℓ'	ℓ					
	3	5	7	9	11	13
1	5.9	0.0	0.0	0.0	0.0	0.0
2	5.9	8.9	0.0	0.0	0.0	0.0
3	7.1	7.3	11.7	0.0	0.0	0.0
4	8.6	7.9	8.6	14.6	0.0	0.0
5	10.1	9.0	8.8	10.0	17.4	0.0
6	11.6	10.1	9.5	9.8	11.4	20.3

Tables 2 and 3 also show that the maxima of both K_ℓ^+ and K_ℓ^- occur for $\ell = 2(\ell' + 1)$. An exception is $\tilde{E}_\ell \tilde{B}_{\ell+1}$ for $\ell' = 2$, where the maximum still occurs at $\ell = 2$. It is important to note that the maximum of $\tilde{E}_\ell \tilde{B}_{\ell-1}$ is much sharper in comparison to the lower ℓ values than that of $\tilde{E}_\ell \tilde{B}_{\ell+1}$. For this reason, we focus our analysis on the former quantity to characterize the spectrum of magnetic helicity, because it serves as the sharpest proxy of the magnetic helicity. Also, the largest contribution to $\tilde{E}_\ell \tilde{B}_{\ell+1}$ has the opposite sign for $\ell \geq 6$.

It is in principle also possible to use $\tilde{B}_{\ell,m}$ itself as a proxy of magnetic helicity. Its values are listed in Table 4 for the same models as above. We emphasize that \tilde{B}_ℓ has contributions only from odd values of ℓ . This is because $B(\theta)$ has a dominant hemispheric $\ell = 1$ variation. By contrast, \tilde{E}_ℓ always has contributions for even values of ℓ . This property of \tilde{E}_ℓ is also

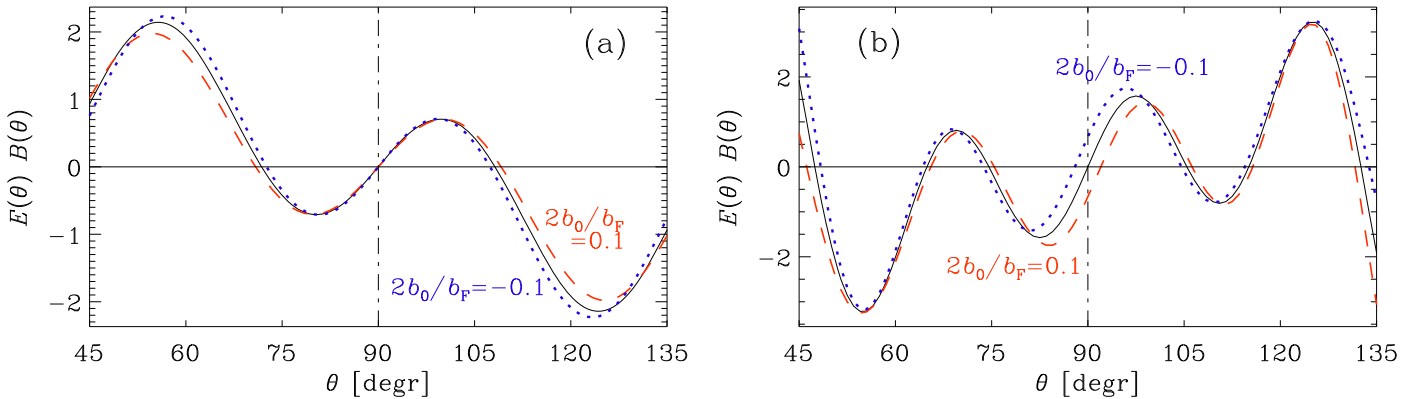


Figure 2. $E(\theta)B(\theta)$ for $b_F = 10$ (red) and -10 (blue) for (a) $l' = 1$ and (b) $l' = 2$. Note that for $l' = 2$, $EB \neq 0$ at the equator ($\theta = 90^\circ$).

recovered if the field is nonhelical, which is the case if the magnetic field is purely poloidal or purely toroidal. On the other hand, if both are present at the same values of ℓ , one has helicity without hemispheric modulation. In that case, \tilde{B}_ℓ has contributions only from even values of ℓ , while \tilde{E}_ℓ vanishes.

2.5. Analogy with Faraday-rotated Fields

Scannapieco & Ferreira (1997) calculated the B mode polarization of the cosmic microwave background radiation in the presence of a uniform magnetic field and found correlations between the temperature at spherical harmonic degree ℓ and the B mode at degrees $\ell + 1$ and $\ell - 1$; see also Scóccola et al. (2004). Such constructs are reminiscent of those in Equation (14). In their case, the uniform magnetic field led to a superposition of Faraday-rotated fields with different angles over the depth near the last scattering surface.

An analogy with Faraday rotation is indeed justified, because both magnetic helicity and Faraday rotation lead to similar effects that, in combination, can either enhance or diminish the resulting polarized intensity (Sokoloff et al. 1998; Brandenburg & Stepanov 2014; Horellou & Fletcher 2014). The presence of magnetic helicity leads either to a correlation or an anticorrelation between the rotation measure and the total polarized intensity (Volegová & Stepanov 2010), depending on whether one looks along or against the direction of the uniform magnetic field. This explains the analogy with the present case, where we have opposite signs of magnetic helicity in the two hemispheres.

To demonstrate the effect of Faraday rotation in the present context, we now include the radial magnetic field. In fact, the poloidal field associated with the latitudinal component $b_\theta = -b_0 P_{\ell'}^1(\cos \theta)$ of our earlier examples implies

$$b_r = (\ell' + 1)b_0 P_{\ell'}(\cos \theta), \quad (15)$$

where $d[\sin \theta P_{\ell'}^1(\cos \theta)]/d \cos \theta = -\ell'(\ell' + 1)P_{\ell'}(\cos \theta)$ has been used, and the $\ell' + 1$ factor follows from Equation (13) and the fact that $-\ell \tilde{a}_\ell/R = b_0$. We consider models with $\ell' = 1$ and 2. Faraday rotation rotates the phase angle of the complex polarization, so Equation (6) has to be replaced by

$$p = -\epsilon(b_\theta + ib_\phi)^2 e^{2ib_r/b_F}, \quad (16)$$

where $b_F = (k_F n_e \lambda^2 d)^{-1}$, with $k_F = 2.6 \times 10^{-17} \text{ G}^{-1}$ being a constant (e.g., Alissandrakis & Chiuderi-Drago 1994), n_e the mean electron density, λ the wavelength, and d the geometrical depth. For example, for $n_e = 10^{14} \text{ cm}^{-3}$, $\lambda = 600 \text{ nm}$, and

$d = 100 \text{ km}$, we have $b_F \approx 10 \text{ kG}$. Since the actual surface magnetic field is much weaker, Faraday rotation will only be a small effect as far as the average field is concerned. However, given that the effect is highly nonlinear, it is usually not negligible in active regions and sunspots.

To assess the effects of Faraday rotation on the resulting EB correlation, it is instructive to look at the latitudinal dependence of the product $E(\theta)B(\theta)$ for two representative cases: one where ℓ' is odd and one where it is even. The result is shown in Figure 2 for $\ell' = 1$ and 2, using $b_0/b_F = \pm 0.1$, and comparing with the case without Faraday rotation. For clarity, we only show the range $45^\circ \leq \theta \leq 135^\circ$. For the Sun, as alluded to above, the actual values of b_0/b_F will be much smaller and the Faraday rotation effect hardly noticeable for the average field.

We see that for $\ell' = 1$, Faraday rotation causes an enhancement (reduction) of the helicity-induced EB correlation if b_F is negative (positive); see Figure 2(a). This agrees qualitatively with the result of Scannapieco & Ferreira (1997), because a uniform magnetic field corresponds to an odd value ℓ' .

For $\ell' = 2$, on the other hand, we have a mixed hemispheric dependence of EB with finite values at the equator. In the case of the Sun, of course, the large-scale magnetic field has odd symmetry around the equator. This also applies to the field within sunspots. The difference between leading and following sunspots would weaken the net effect, but not its systematic north–south dependence. We can therefore conclude that Faraday rotation does not compromise the ability to detect magnetic helicity from EB , provided the Faraday effect remains subdominant compared with the helicity effect, i.e., λ is small enough.

3. Nonaxisymmetric Examples

3.1. Two-dimensional Patterns of E and B

We now consider two-dimensional examples in the (ϕ, μ) plane, where $\mu = \cos \theta$. Analogous to earlier work, we consider the magnetic field $(b_\phi, b_\mu) \equiv (b_\phi, -b_\theta)$ to be given by $\mathbf{b} = \mathbf{F} + \mathbf{G}$, where

$$F_i = \nabla_i f \quad \text{and} \quad G_i = \epsilon_{ij} \nabla_j g, \quad (17)$$

using

$$f = -f_0 Y_{\ell m} \quad \text{and} \quad g = g_0 Y_{\ell m}. \quad (18)$$

The complex linear polarization is then computed as $p = -(b_\theta + ib_\phi)^2 = (b_\phi - ib_\theta)^2 = (b_\phi + ib_\mu)^2$.

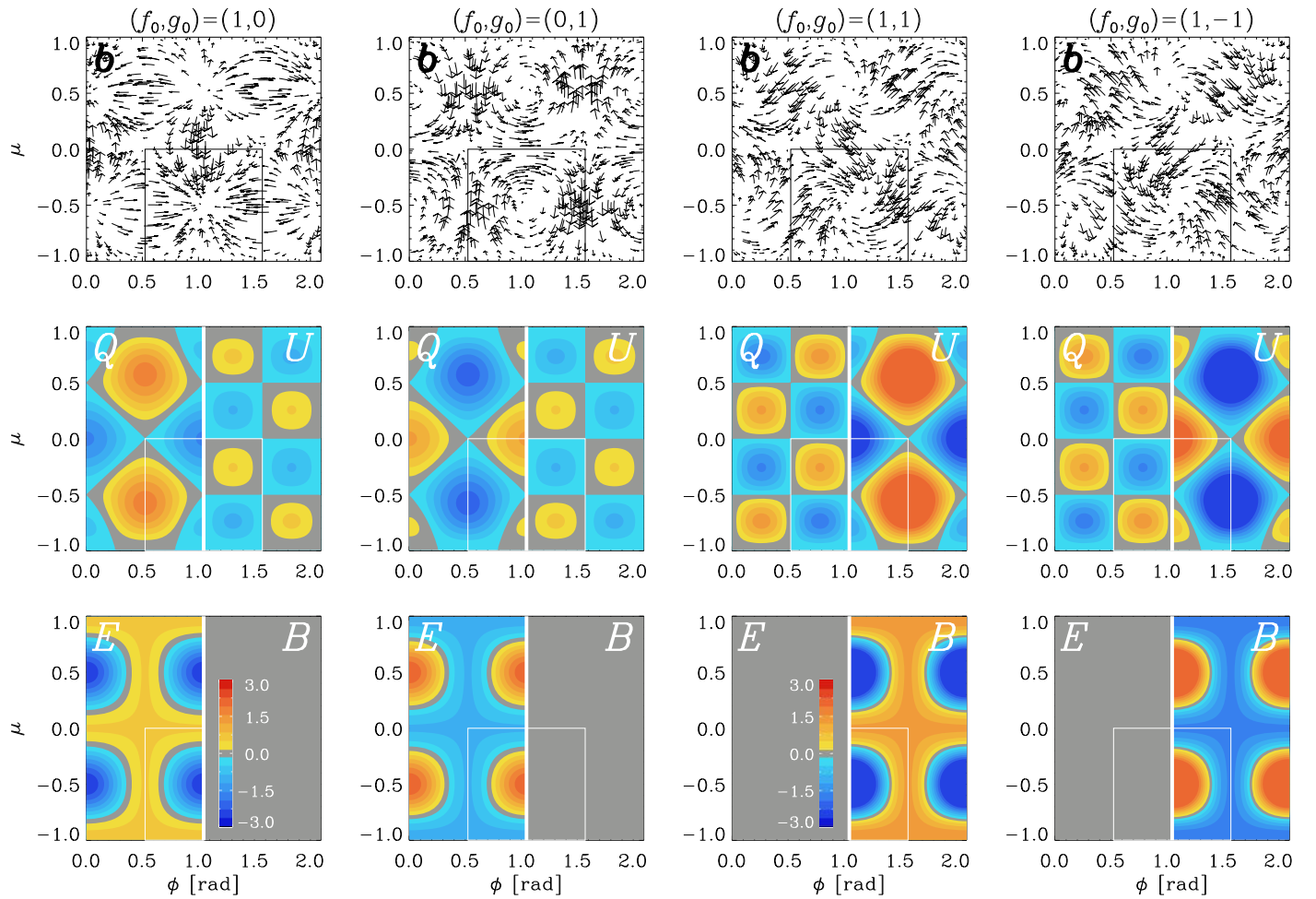


Figure 3. $b(\phi, \mu)$ vectors compared with split representations of (Q, U) and (E, B) for the four combinations $(f_0, g_0) = (1, 0), (0, 1)$, and $(1, \pm 1)$ with $\ell = 4$ and $m = 3$. Individual cross, ring, and swirl-like patterns are highlighted by squares, along with their positions in the (Q, U) and (E, B) diagrams.

Following BBKMRPS, we consider four combinations, namely $(f_0, g_0) = (1, 0), (0, 1)$, and $(1, \pm 1)$. In Figure 3, we show the result for $\ell = 4$ and $m = 3$. All quantities are plotted as a function of ϕ and $\mu = \cos \theta$. This corresponds to the Lambert azimuthal equal-area projection. We recover familiar structures corresponding to star-like and ring-like features for negative and positive E polarizations and swirl-like inward clockwise and counter-clockwise patterns for negative and positive B polarizations. These structures agree with those in Figure 2 of BBKMRPS. We recall, however, that we follow here the sign convention of Durrer (2008), in which our Equation (11) becomes $\tilde{R}(k_x, k_y) = -(\hat{k}_x - i\hat{k}_y)^2 \tilde{p}(k_x, k_y)$ in the Cartesian limit, where k_x and k_y are the components of the two-dimensional wavevector and hats indicate unit vectors. Equation (3) of BBKMRPS, followed the sign convention of Zaldarriaga & Seljak (1997), but their Figure 2 showed polarization vectors, which are at right angles to the magnetic field vectors, therefore giving the same orientation as the magnetic vectors in the Durrer convention shown in our Figure 3.

3.2. Formulation in Terms of Superpotentials

Nonaxisymmetric magnetic fields can no longer be expressed in a form analogous to Equation (1), but we must

instead employ the superpotentials S and T in the form

$$\mathbf{b} = \nabla \times \nabla \times (\mathbf{r}S) + \nabla \times (\mathbf{r}T). \quad (19)$$

The first part corresponds to the poloidal field and the second to the toroidal field. The two superpotentials are expanded in terms of spherical harmonics, so

$$(S, T)(\theta, \phi) = \sum_{\ell=1}^{N_\ell} \sum_{m=-\ell}^{\ell} (S_{\ell m}, T_{\ell m}) Y_{\ell m}(\theta, \phi), \quad (20)$$

with the inverse transformation given by

$$(\tilde{S}_{\ell m}, \tilde{T}_{\ell m}) = \int_{4\pi} (S, T)(\theta, \phi) Y_{\ell m}^*(\theta, \phi) \sin \theta d\theta d\phi. \quad (21)$$

As in Section 2.1, we assume that the radial dependence of $\tilde{S}_{\ell m}(r)$ is proportional to $r^{-(\ell+1)}$. This implies that

$$\frac{\partial}{\partial r}(r \tilde{S}_{\ell m}) = -\ell \tilde{S}_{\ell m} \quad (\text{for } r = R). \quad (22)$$

For chosen values of ℓ and m , we can then write

$$b_\theta(\theta, \phi) = \text{Re}(-\ell \tilde{S}_{\ell m} \nabla_\theta Y_{\ell m} + \tilde{T}_{\ell m} \nabla_\phi Y_{\ell m}), \quad (23)$$

$$b_\phi(\theta, \phi) = \text{Re}(-\ell \tilde{S}_{\ell m} \nabla_\phi Y_{\ell m} - \tilde{T}_{\ell m} \nabla_\theta Y_{\ell m}). \quad (24)$$

Note in this connection that for axisymmetric models, b_θ and b_ϕ are related to $Y_{\ell m}(\theta, \phi)$ via θ derivatives. This shows that the reason for having expanded $a_\phi(\theta)$ and $b_\phi(\theta)$ in Equation (2) in

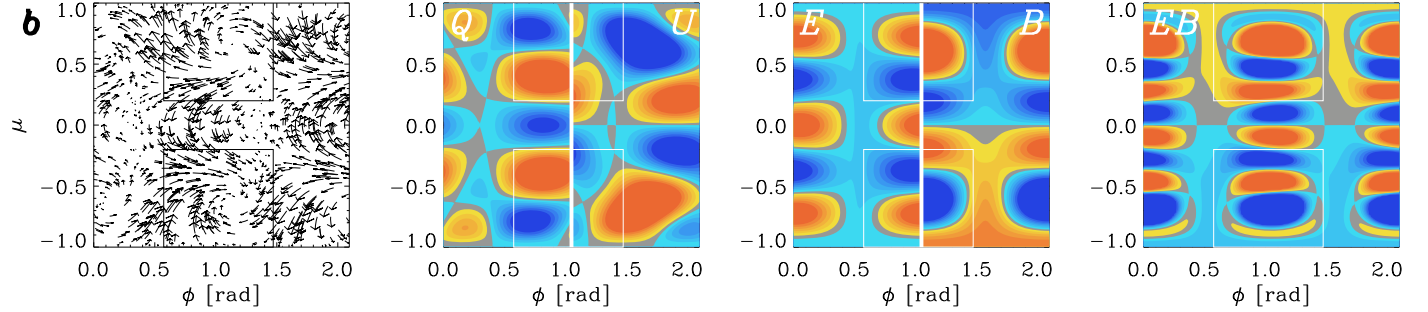


Figure 4. $b(\phi, \mu)$ vectors compared with split representations of (Q, U) and (E, B) , and a representation of the product EB , for the model of Section 3.3 with $\ell = 4$ and $m = 3$. Note the opposite sense of swirl of eddies in the northern and southern hemispheres, as highlighted by the squares.

terms of $P_\ell^1(\cos \theta)$ is that the θ derivative of the Legendre polynomials gives $dP_\ell(\cos \theta)/d\theta = P_\ell^1(\cos \theta)$. Analogously to the axisymmetric case, we choose $\tilde{T}_{\ell m} = -\ell \tilde{S}_{\ell m}/R = b_0 R$.

The formulation given by Equations (23) and (24) agrees with that given by Equation (17), provided we replace

$$f \rightarrow -\ell \tilde{S}_{\ell m} Y_{\ell m}(\theta, \phi), \quad g \rightarrow \tilde{T}_{\ell m} Y_{\ell m}(\theta, \phi). \quad (25)$$

This formulation suggests that the nonaxisymmetric generalization of Equation (5) is given by

$$f \rightarrow -\ell' \tilde{S}_{\ell' m'} Y_{\ell' m'} R, \quad g \rightarrow \tilde{T}_{\ell'+1 m'} Y_{\ell'+1 m'}, \quad (26)$$

and that

$$H_{\ell'}^\pm = \sum_{m'=-\ell'}^{\ell'} 2\ell'(\ell' + 1) \tilde{S}_{\ell' m'} \tilde{T}_{\ell' \pm 1 m'}^* \quad (27)$$

can be used as a global two-scale measure of the magnetic helicity spectrum. In the following, we use $H_{\ell' m'}^+$ to specify the amplitude of a single mode; $H_{\ell' m'}^-$, by contrast, vanishes in our single-mode examples by construction. We also use H_ℓ^+ for solar magnetograms.

3.3. Hemispheric Helicity Modulation

In the examples considered above, either E or B was zero; see the gray sub-panels in the split representation of Figure 3. We now consider examples where both are nonvanishing. Specifically, we reconstruct examples where

$$K_\ell^\pm \equiv \sum_{m=-\ell}^{\ell} \tilde{E}_{\ell m} \tilde{B}_{\ell \pm 1 m}^* \quad (28)$$

is nonvanishing. As noted in the previous section, we do this by using fields where

$$-\ell' \tilde{S}_{\ell' m'} / R = \tilde{T}_{\ell'+1 m'} = -b_0 \quad (29)$$

is a constant for fixed ℓ' and m' . This is equivalent to our choice $-\ell' \tilde{a}_{\ell'} / R = \tilde{b}_{\ell'+1} = b_0$ in Section 2.4. Furthermore, the models of Figure 1 correspond to $(f_0, g_0) = (1, -1) \times 4\pi/\sqrt{(2\ell+1)(2\ell+3)}$. The result is shown in Figure 4, again for $\ell = 4$ and $m = 3$. We see that E is always symmetric about the equator and B is antisymmetric about the equator. The product EB is therefore antisymmetric about the equator, which reflects the opposite signs of magnetic helicity in the two hemispheres.

The last panel of Figure 4 shows that, although the product EB is mostly positive in the north and negative in the south, there are also extended regions of opposite sign. Quantitatively,

Table 5
Values of $\tilde{E}_{\ell m}$, $\tilde{B}_{\ell-1 m}$, and $\tilde{E}_{\ell m} \tilde{B}_{\ell-1 m}$ for $\ell = 4$ and $m' = 3$

ℓ	2	4	6	8	10
$\tilde{E}_{\ell=0}$	1.00	-0.37	-2.61	2.43	-0.63
$\tilde{B}_{\ell=1,0}$	0	-2.37	-3.14	3.25	-0.82
$\tilde{E}_{\ell=0} \tilde{B}_{\ell=10}^*$	0	0.89	8.19	7.88	0.51
$\tilde{E}_{\ell=6}$	0	0	$0.33 - 0.52i$	$-0.19 - 0.15i$	1.94
$\tilde{B}_{\ell=16}$	0	0	0	1.67	3.18
$\tilde{E}_{\ell=6} \tilde{B}_{\ell=16}^*$	0	0	0	$-0.31 - 0.24i$	6.19
K_ℓ^-	0	0.89	8.19	7.26	12.89
$\sum \tilde{E}_{\ell m} ^2$	1.00	0.14	7.57	6.02	7.92
$\sum \tilde{B}_{\ell-1 m} ^2$	0	5.62	9.86	16.1	20.90
$c_A(\ell)$	0	0.31	0.94	0.66	0.89

we find that $2\langle EB \rangle / \langle E^2 + B^2 \rangle = \pm 0.25$, where the upper (lower) sign applies to the northern (southern) hemisphere.

In Table 5, we list all nonvanishing coefficients $\tilde{E}_{\ell m}$ and $\tilde{B}_{\ell m}$ for our example with $\ell' = 4$ and $m' = 3$. For $m \neq 0$, the only nonvanishing contributions come from $m = \pm 6$. Note also that $\tilde{E}_{\ell m}$ is now complex, while all other coefficients are still real. The dominant contributions to the parity-odd correlation come from the product $\tilde{E}_{\ell m} \tilde{B}_{\ell-1 m}$ with $\ell = 2(\ell' - 1) = 6$ and $\ell = 2\ell' = 8$ for $m = 0$, and $\ell = 2(\ell' + 1) = 10$ for $m = 2m' = 6$.

4. Solar Synoptic Vector Magnetograms

4.1. Spectra of Global Two-scale Helicity Proxies

We now apply the global two-scale approach to the same solar synoptic vector magnetograms that were studied by BPS using the semi-global approach. As alluded to in the introduction, we use “ π -ambiguated” magnetic fields expressed in terms of pseudo-polarization data. Thus, we only utilize the two horizontal components, b_θ and b_ϕ , to compute the complex linear polarization $p(\theta, \phi) = -(b_\theta + ib_\phi)^2$. The emissivity prefactor in Equation (6) has been set to unity because, in the following, we only work with normalized spectra. We then compute $\tilde{E}_{\ell m}$ and $\tilde{B}_{\ell m}$ and study the spectra K_ℓ^\pm ; see Equation (28). We normalize them analogously to those in BBKMRPS and write them as

$$c_A^\pm(\ell) = \frac{\sum_{m=-\ell}^{\ell} 2\tilde{E}_{\ell m} \tilde{B}_{\ell \pm 1 m}^*}{\sum_{m=-\ell}^{\ell} (|\tilde{E}_{\ell m}|^2 + |\tilde{B}_{\ell \pm 1 m}|^2)}. \quad (30)$$

Because we sum over positive and negative m , the values of $c_A^\pm(\ell)$ are always real. They vary between -1 and $+1$. We recall that, based on the comparison of Tables 2 and 3 in Section 2.4,

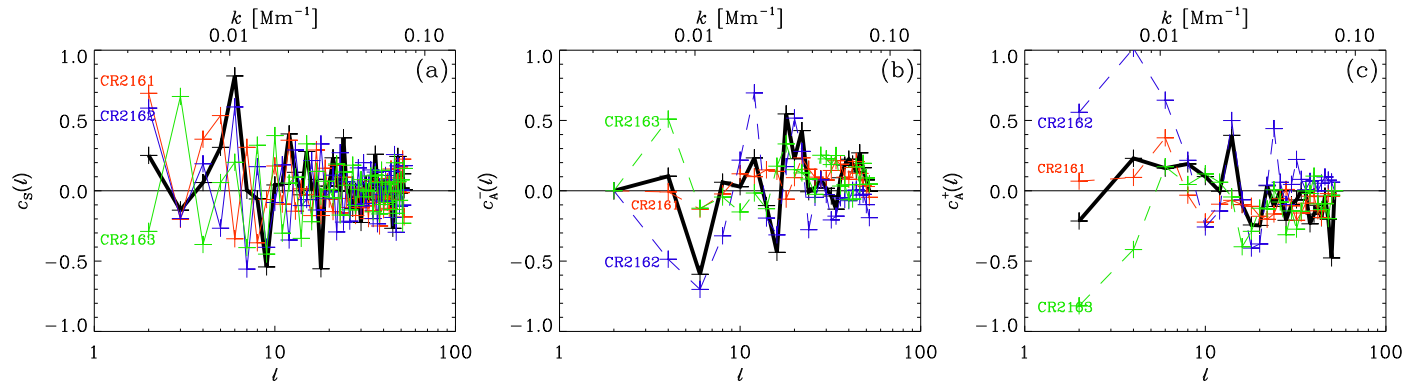


Figure 5. (a) $c_S(\ell)$, (b) $c_A^- (\ell)$, and (c) $c_A^+ (\ell)$ for the full data set covering CRs 2161–2163 (broad solid lines), compared with the corresponding individual results for CRs 2161 (red), 2162 (blue), and 2163 (green).

we expect $c_A^- (\ell)$ to be a better proxy of magnetic helicity than $c_A^+ (\ell)$.

Following BBKMRPS, we also compute the normalized difference of the spectra of *EE* and *BB* polarizations as

$$c_S(\ell) = \frac{\sum_{m=-\ell}^{\ell} (|\tilde{E}_{\ell m}|^2 - |\tilde{B}_{\ell m}|^2)}{\sum_{m=-\ell}^{\ell} (|\tilde{E}_{\ell m}|^2 + |\tilde{B}_{\ell m}|^2)}. \quad (31)$$

This quantity varies between -1 and $+1$. It vanishes when the *EE* and *BB* polarizations have the same amplitude, and it is one third if the amplitude of the *EE* polarization is twice that of the *BB* polarization, as was found in recent dust foreground measurements of the interstellar medium (Planck Collaboration Int. XXX 2016; Planck Collaboration results XI 2018). To facilitate comparison with earlier work, we define

$$L^2 = \ell(\ell + 1), \quad (32)$$

and plot c_S and c_A^\pm also versus the approximate wavenumber $k = L/R$. As in BPS, we use the combined synoptic vector magnetograms of three CRs, 2161, 2162, and 2163. They are based on the full-disk vector magnetograms obtained from the Helioseismic and Magnetic Imager on board the *Solar Dynamics Observatory* and have been processed by Yang Liu⁵ (Stanford).

In Figure 5, we show $c_S(\ell)$ and $c_A^\pm(\ell)$ both for the full data set of all three CRs and also separately for CRs 2161, 2162, and 2163. For the full data set, the total azimuthal angle is 6π , and the integration in Equation (11) is carried out over 12π instead of 4π . Similar to our earlier semi-global analysis, c_S shows large variations, but is mostly positive for $\ell \leq 10$, corresponding to the wavenumber $k = L/R \leq 0.014 \text{ Mm}^{-1}$. Furthermore, c_A^- shows negative values for similar ℓ , while c_A^+ has the opposite sign, which is in agreement with our expectations based on the comparison of Tables 2 and 3. For larger ℓ , both c_A^+ and c_A^- are again very noisy, although c_A^- may be mostly positive, while c_A^+ may be mostly negative.

To have an estimate of the uncertainty of our results, we also plot the spectra separately for each of the three CRs. These results are broadly consistent with those of the full data set. The tendency of obtaining positive values of c_S at $\ell < 10$ is also seen individually for all three CRs. By contrast, the tendency of obtaining negative values of c_A^- for $\ell < 10$ is seen for CRs 2161 and 2162, but not for CR 2163 at $\ell = 4$. However,

for $\ell = 6$, all three data sets give the same (negative) sign of c_A^- .

As noted before, \tilde{B}_ℓ can itself be used as a helicity proxy, so we now determine it for the same three CRs. For completeness, we also analyze \tilde{E}_ℓ in a similar fashion. Owing to nonaxisymmetry, we have contributions from different values of m . It is then useful to define

$$\tilde{B}_\ell = \sum_{m=-\ell}^{\ell} \tilde{B}_{\ell m}, \quad \tilde{B}_\ell^{(2)} = \sum_{m=-\ell}^{\ell} |\tilde{B}_{\ell m}|^2. \quad (33)$$

In the following, we plot \tilde{B}_ℓ and the ratio $\tilde{B}_\ell/\tilde{B}_\ell^{\text{rms}}$, where $\tilde{B}_\ell^{\text{rms}} = [\tilde{B}_\ell^{(2)}]^{1/2}$ is the rms value. We define \tilde{E}_ℓ and the ratio $\tilde{E}_\ell/\tilde{E}_\ell^{\text{rms}}$ analogously. For \tilde{B}_ℓ , we only expect to see a hemispheric modulation for odd values of ℓ . Therefore, to distinguish the contributions from odd and even values of ℓ , we denote them as $\tilde{B}_\ell^{\text{odd}}$ and $\tilde{B}_\ell^{\text{even}}$. The results are shown in Figure 6 as a function of ℓ . We see that both \tilde{E}_ℓ and $\tilde{B}_\ell^{\text{odd}}$ are negative for small values of ℓ , while $\tilde{B}_\ell^{\text{even}}$ is positive.

The fact that \tilde{E}_ℓ is mostly negative for $\ell < 5$ suggests that, on large length scales, the magnetic field structures are mostly star-like, but in the range $5 < \ell < 10$, they are mostly ring-like. However, no direct visual evidence of this has been reported as yet. For the *B* polarization, on the other hand, the negative values for odd ℓ , i.e., for $\tilde{B}_\ell^{\text{odd}}$, may reflect a positive magnetic helicity on large length scales; see Section 3.3. This agrees with the negative sign found for c_A^- . Moreover, as seen in Table 2, K_ℓ^+ tends to have the opposite sign. This agrees with what is found for c_A^+ in Figure 5(c).

4.2. Spectra of the Global Two-scale Magnetic Helicity

Finally, we consider H_ℓ^\pm . We normalize it by the solar radius R , which is set to unity in our work, so we plot here the ratio H_ℓ^\pm/R , which has units of G^2 ; see Equation (27) for the definition. To obtain $\tilde{S}_{\ell m}$, we use the observed radial magnetic field component, b_r , compute the spherical harmonics decomposition to find $\tilde{b}_{r,\ell m}$ and thus $\tilde{S}_{\ell m} = \tilde{b}_{r,\ell m}/L^2$; see Equation (32). Analogously, we compute $\tilde{T}_{\ell m}$ from the radial component of the current density, j_r . For the vector magnetograms, the components of the magnetic field are given in uniform intervals of $\mu = \cos \theta$. We therefore write the radial

⁵ <http://hmi.stanford.edu/hminuggets/?p=1689>

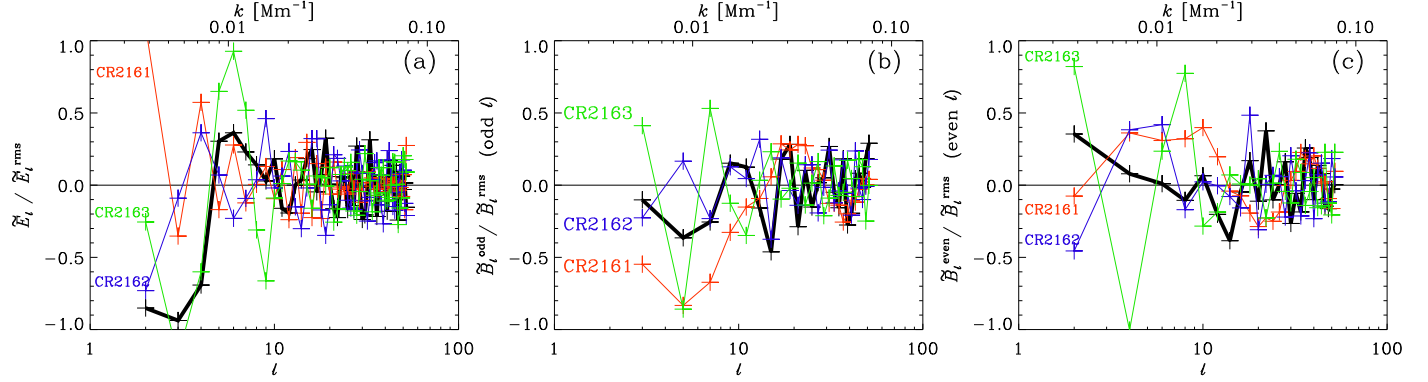


Figure 6. (a) $\tilde{E}_\ell / \tilde{E}_{\ell}^{\text{rms}}$ (for even and odd ℓ), (b) $\tilde{B}_\ell^{\text{odd}} / \tilde{B}_{\ell}^{\text{rms}}$ (only for odd values of ℓ), and (c) $\tilde{B}_\ell^{\text{even}} / \tilde{B}_{\ell}^{\text{rms}}$ (for even values of ℓ), for the full data set covering CRs 2161–2163 (broad solid lines), compared with the corresponding individual results for CRs 2161 (red), 2162 (blue), and 2163 (green).

component of $\mathbf{j} = \nabla \times \mathbf{b}$ as

$$j_r = \cot \theta b_\phi - \sin \theta \frac{\partial b_\phi}{\partial \mu} - \frac{1}{\sin \theta} \frac{\partial b_\theta}{\partial \phi}. \quad (34)$$

We then compute the spherical harmonics decomposition to find $\tilde{j}_{r,\ell m}$ and thus compute $\tilde{T}_{\ell m} = \tilde{j}_{r,\ell m} / L^2$.

In Figure 7 we plot H_ℓ^\pm / R versus ℓ . We see that H_ℓ^+ and H_ℓ^- are negative for most values of ℓ . Thus, there is no clear evidence for a positive magnetic helicity at large length scales. This is surprising in view of the previous findings based on the B polarization that did suggest positive magnetic helicity on large length scales. Of course, previous work has long shown negative magnetic helicity in the northern hemisphere and positive in the southern (Seehafer 1990; Pevtsov et al. 1995), including the work of BPS. It may therefore indeed be true that there is no sign change in H_ℓ^\pm at the photosphere, and that the sign change in the helicity proxies may reflect physical properties of the field at some layer above the photosphere. However, it could also be an effect of the phase within the solar cycle, as suggested by Singh et al. (2018), which could then also explain the evidence for a bihelical field found by Pipin & Pevtsov (2014). Systematic cycle related magnetic helicity variations are indeed well documented (Kleeorin et al. 2003; Zhang et al. 2010; Pipin et al. 2019).

It also is surprising that H_ℓ^\pm is, for all CRs, consistently much larger at $\ell = 1$ than for any other values of ℓ . In BPS, by contrast, we found a rapid decline of power for 0.01 Mm^{-1} ; see Figure 8 therein, but that work was based on a semi-global approach which is unable to recover the low k values correctly. Conversely, it is possible that the global approach over-emphasizes the polar fields. This may be a concern mainly for the E and B polarization. Indeed, looking at Figure 1, we see that the clearest hemispheric dependence in B is seen at the poles, while at lower latitudes, E and B have no definite correlation. This may well be a general problem with the EB approach that should be clarified studying the signs of E and B locally. It would be important to assess the statistical robustness of these results by inspecting the magnetic helicity signatures for many more CRs.

5. Implications for Dynamo Theory

The α effect in dynamo theory is the main candidate for explaining the production of large-scale magnetic fields in the Sun. One of its signatures is the production of magnetic helicity of opposite signs. Such a magnetic field is called bihelical.

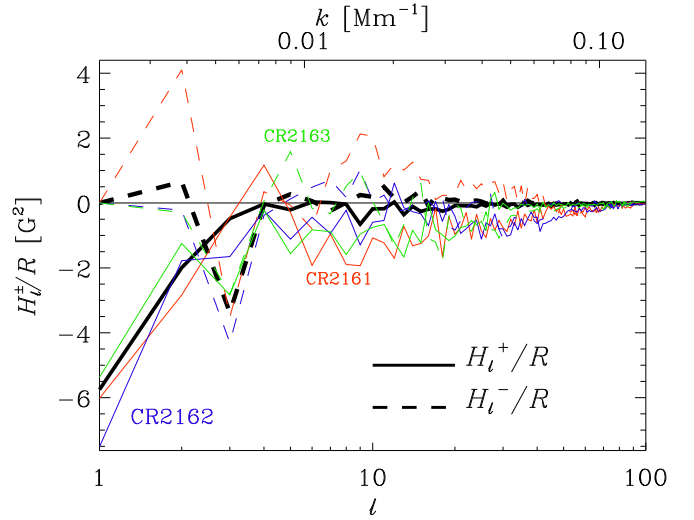


Figure 7. H_ℓ^\pm / R vs. ℓ for the full data set covering CRs 2161–2163 (broad solid lines), compared with the corresponding individual results for CRs 2161 (red), 2162 (blue), and 2163 (green). The solid (dashed) lines give the results for odd (even) values of ℓ .

Figures 5 and 6 present some support for this assertion, in addition to the earlier results of Pipin & Pevtsov (2014) and Singh et al. (2018). Our inspection of H_ℓ^+ and H_ℓ^- does not support this, however. Whether this is indeed related to potential problems regarding the π ambiguity is, however, unclear, and one would like to see more evidence before continuing to speculate further on this. There is, however, the possibility that it might be related to the anticipated sign reversal of magnetic helicity some small distance above the photosphere. We elaborate on this possibility next.

To put the various findings into a broader perspective, it is important to realize that in the solar wind, far away from the solar dynamo, evidence for a bihelical magnetic field has also been presented (Brandenburg et al. 2011). However, the sign of magnetic helicity is at all wavenumbers opposite to what it is at the solar surface. This was then found to be a generic phenomenon of any system consisting of a dynamo region adjacent to a nondynamo region; see the work of Warnecke et al. (2011, 2012) of a turbulent dynamo simulation with a simple stellar corona, and the earlier work of Brandenburg et al. (2009) in the context of galactic halos. We do not know exactly where the sign would swap. It has been suggested that it could occur in the lower corona, where the plasma beta crosses unity

(Bourdin et al. 2018). This could be detectable by measuring in situ polarized emission from within the corona (Brandenburg et al. 2017a). On the other hand, if it happened in the chromosphere, in layers accessible to a direct face-on measurement of the EB cross-correlation, this sign change might be detectable using the method discussed in the present paper.

A major difficulty in detecting an overall sign change of handedness through the EB cross-correlation lies in the fact that the E polarization is strongly associated with the magnetic field topology. This particular property could be characterized, for example, by its correlation with temperature T (related to the intensity or Stokes I). This is a parity-even correlation, which can have either sign, and it may be this quantity, in addition to EB , that also shows a systematic variation with height. Not much is known about this, except that in the dust polarization of the Galactic foreground, the ET correlation is known to be positive (Planck Collaboration results XI 2018). We also know that the E polarization is highly skewed and its skewness depends systematically on the physics governing the magnetic field. Ambipolar diffusion, for example, is known to affect the skewness of E in a systematic way (see Figure 13 of Brandenburg 2019). This is also reflected in the fact that the EE correlation can be different from the BB correlation, i.e., $c_S \neq 0$, as has been found in the present work; see Figure 5(a). Addressing these new questions raised above is of direct relevance to assessing the possibility of a radial sign reversal of the magnetic helicity, as predicted by dynamo theory and as has been found from magnetic helicity measurements in the solar wind.

6. Conclusions

This work has addressed two critical issues in the calculation of a proxy of solar magnetic helicity spectra: the π ambiguity and the systematic north–south sign change of magnetic helicity. The problem of the π ambiguity has been addressed previously (BBKMRPS) by calculating the EB cross-correlation from local Cartesian patches. This quantity was shown to be a proxy of magnetic helicity under inhomogeneous conditions, in particular for rotating stratified convection. The problem of the systematic north–south variation has also been addressed previously, but only in a semi-global fashion; see BPS. Here, we have generalized this approach to a fully global one by first calculating the parity-even and parity-odd E and B polarizations globally using spin-2 spherical harmonics, and then correlating them at spherical harmonic degrees that are shifted by one relative to the other. This approach is analogous to what was done in the semi-global Cartesian approach of BPS. However, unlike their formalism, the present one is heuristic and has not been derived rigorously from a correlation function that depends on mean and relative coordinates; see Roberts & Soward (1975). It is not entirely obvious that this is even possible but, if it is, the result may well look similar to what has been proposed here. Through the examples constructed here, we have demonstrated that the correlation $\tilde{E}_{\ell m} \tilde{B}_{\ell-1m}^*$ can act as a proxy of the magnetic helicity, which itself is characterized globally by the product $\tilde{S}_{\ell m} \tilde{T}_{\ell+1m}^*$.

In the quest for finding clear evidence of an opposite sign of magnetic helicity at large length scales, one has to tackle the problem of the π ambiguity in the weak-field regions that occupy the majority of the solar surface. A standard approach

to π disambiguation in those regions is the random disambiguation, which is problematic and may have been responsible for the relatively low spectral power at wavenumbers around and below 0.03 Mm^{-1} (Singh et al. 2018) and also for what looked like a random sign in the resulting magnetic helicity at those wavenumbers. In fact, the present results now suggest that there is maximum power at the very smallest wavenumbers around and below 0.01 Mm^{-1} .

Our results show that, in the northern hemisphere, where the small-scale magnetic helicity is negative, $\tilde{E}_{\ell m} \tilde{B}_{\ell-1m}^*$ is positive. Likewise, the large-scale field is expected to have positive magnetic helicity in the northern hemisphere and $\tilde{E}_{\ell m} \tilde{B}_{\ell-1m}^*$ is now found to be negative. Thus, our proxy has the opposite sign to the magnetic helicity. This agrees with what was found based on the numerical simulations of BBKMRPS. This result is not, however, based on the actual helicity H_ℓ^\pm , but rather on the helicity proxy. As mentioned in Section 4.2, there could be a general difficulty with the EB approach in that its highest sensitivity is at the poles. At lower latitudes, the method suffers a significant amount of cancellation, as can be anticipated from Figure 1 for $\ell = 4$.

Regarding the absence of a clear EB signal in the analysis of solar Q and U polarization in the work of BBKMRPS, it should be noted that their results are much more noisy, although in hindsight not so dissimilar from the present ones. Tentatively, they found values at small and large length scales that agree with those here: positive $c_S(k)$ at $k = 0.01 \text{ Mm}^{-1}$ along with $c_A(k)$ at similar values of k . However, the main reason for their noisy result lies probably in the fact that their linear polarization data were too contaminated by other factors, as was already discussed in BBKMRPS.

The present approach of computing the EB signal from the magnetic field rather than the observed polarization combines the best aspects of two worlds. It uses the elaborate inversion technique of spectropolarimetry to obtain the magnetic field, but is insensitive to the problems associated with the π ambiguity. What is perhaps unsatisfactory, however, is the fact that the line-of-sight magnetic field (b_{\parallel}) or the circular polarization are not used in the present approach. No corresponding idea has yet been proposed that would combine these two pieces of information. Simply correlating b_{\parallel} with E or B may not yield anything useful because in simple patterns such as those of Figure 3, the wavelength of b_{\parallel} is always twice that of E or B , so it would lead to a cancellation. This is because E and B are related to the square of the magnetic field. Therefore, the spatial wavelengths of the E and B patterns would agree with that of b_{\parallel}^2 , but then the potentially useful information implied by the sign of b_{\parallel} is lost. So, it is not obvious what to do with b_{\parallel} in this context.

In this connection, it is useful to remind ourselves that, away from disk center, b_{\parallel} does begin to contribute more strongly to the determination of b_θ and b_ϕ . One should therefore calculate the complex polarization not from b_θ and b_ϕ , but from the two components of the field vector \mathbf{b}_\perp that is perpendicular to the line of sight. This would obviously be another next important step to take. Likewise, it would be highly valuable to inspect the spatial properties of E and B in much more detail. This would allow us to study the connection between the sign of E and the topology or structures, and of course between the sign of B and the hemispheric position.

One of the other potential applications of the EB transformation lies in its potential benefit when regularizing the observed

linear polarization signal. One could imagine that, instead of applying a random disambiguation for weak field strengths, one could adopt some type of image reconstruction in EB space instead of working in QU or b space. This has not yet been explored and would be a useful target for future research.

Finally, one may wonder whether the global two-scale helicity proxy introduced here can be used beyond solar physics. The answer is probably yes, if one thinks about the technique of Zeeman Doppler imaging of stellar magnetic fields (see, e.g., Donati et al. 1997; Carroll et al. 2012; Rosén et al. 2015). Likewise, the magnetic field of our own Galaxy may also be subject to such an analysis (Jansson & Farrar 2012). We therefore expect that these points provide exciting opportunities for future work.

This work was carried out in large parts at the Aspen Center for Physics, which is supported by National Science Foundation grant PHY-1607611. I thank Evan Scannapieco for organizing the Aspen program on the Turbulent Life of Cosmic Baryons. I also thank Gherardo Valori and Etienne Pariat for organizing the Magnetic Helicity in Astrophysical Plasmas Team at the International Space Science Institute in Bern, where some early elements of this work were conceived, and I also thank Maarit Käpylä Alexei Pevtsov, Ilpo Virtanen, and Nobumitsu Yokoi for providing a splendid atmosphere at the Nordita program on Solar Helicities in Theory and Observations. I am grateful to Patrik Sanila for help with the spin-weighted spherical harmonics, and to Ameya Prabhu for showing me some of his preliminary results with π -ambiguated magnetic fields using local patches around specific active regions. I also thank Marc Kamionkowski and Kandaswamy Subramanian for useful discussions on the subject, and an anonymous referee for suggesting improvements to the paper. This research was supported in part by the Astronomy and Astrophysics Grants Program of the National Science Foundation (grant 1615100), and the University of Colorado through its support of the George Ellery Hale visiting faculty appointment. I acknowledge the allocation of computing resources provided by the Swedish National Allocations Committee at the Center for Parallel Computers at the Royal Institute of Technology in Stockholm.

ORCID iDs

Axel Brandenburg  <https://orcid.org/0000-0002-7304-021X>

References

Alissandrakis, C. E., & Chiuderi-Drago, F. 1994, *ApJL*, 428, L73

- Blackman, E. G., & Brandenburg, A. 2003, *ApJS*, 84, L99
 Bourdin, Ph.-A., Singh, N. K., & Brandenburg, A. 2018, *ApJ*, 869, 3
 Bracco, A., Candelaresi, S., Del Sordo, F., & Brandenburg, A. 2019, *A&A*, 621, A97
 Brandenburg, A. 2019, *MNRAS*, 487, 2673
 Brandenburg, A., Ashurova, M. B., & Jabbari, S. 2017a, *ApJL*, 845, L15
 Brandenburg, A., Bracco, A., Kahnashvili, T., et al. 2019, *ApJ*, 870, 87, (BBKMRPS)
 Brandenburg, A., Candelaresi, S., & Chatterjee, P. 2009, *MNRAS*, 398, 1414
 Brandenburg, A., Dobler, W., & Subramanian, K. 2002, *AN*, 323, 99
 Brandenburg, A., Petrie, G. J. D., & Singh, N. K. 2017b, *ApJ*, 836, 21, (BPS)
 Brandenburg, A., & Stepanov, R. 2014, *ApJ*, 786, 91
 Brandenburg, A., Subramanian, K., Balogh, A., & Goldstein, M. L. 2011, *ApJ*, 734, 9
 Carroll, T. A., Strassmeier, K. G., Rice, J. B., & Küntler, A. 2012, *A&A*, 548, A95
 Donati, J.-F., Semel, M., Carter, B. D., Rees, D. E., & Collier Cameron, A. 1997, *MNRAS*, 291, 658
 Durrer, R. 2008, The Cosmic Microwave Background (Cambridge: Cambridge Univ. Press)
 Georgoulis, M. K. 2005, *ApJL*, 629, L69
 Goldberg, J. N., Macfarlane, A. J., Newman, E. T., Rohrlich, F., & Sudarshan, E. C. G. 1967, *JMP*, 8, 2155
 Hoeksema, J. T., Liu, Y., Hayashi, K., et al. 2014, *SoPh*, 289, 3483
 Horellou, C., & Fletcher, A. 2014, *MNRAS*, 441, 2049
 Hughes, A. L. H., Bertello, L., Marble, A. R., et al. 2016, arXiv:1605.03500
 Jansson, R., & Farrar, G. R. 2012, *ApJ*, 757, 14
 Kahnashvili, T., Maravin, Y., Lavrelashvili, G., & Kosowsky, A. 2014, *PhRvD*, 90, 083004
 Kahnashvili, T., & Ratra, B. 2005, *PhRvD*, 71, 103006
 Kamionkowski, M., Kosowsky, A., & Stebbins, A. 1997, *PhRvL*, 78, 2058
 Kamionkowski, M., & Kovetz, E. D. 2016, *ARA&A*, 54, 227
 Kleedorin, N., Kuzanyan, K., Moss, D., et al. 2003, *A&A*, 409, 1097
 Krause, F., & Rädler, K.-H. 1980, Mean-field Magnetohydrodynamics and Dynamo Theory (Oxford: Pergamon)
 Liu, Y., Hoeksema, J. T., Sun, X., & Hayashi, K. 2017, *SoPh*, 292, 29
 Pevtsov, A. A., Canfield, R. C., & Metcalf, T. R. 1995, *ApJL*, 440, L109
 Pipin, V. V., & Pevtsov, A. A. 2014, *ApJ*, 789, 21
 Pipin, V. V., Pevtsov, A. A., Liu, Y., & Kosovichev, A. G. 2019, *ApJL*, 877, L36
 Planck Collaboration Int. XXX 2016, *A&A*, 586, A133
 Planck Collaboration results XI 2018, *A&A*, arXiv:1801.04945
 Roberts, P. H., & Soward, A. M. 1975, *AN*, 296, 49
 Rosén, L., Kochukhov, O., & Wade, G. A. 2015, *ApJ*, 805, 169
 Rudenko, G. V., & Anfinogentov, S. A. 2014, *SoPh*, 289, 1499
 Sakurai, T., Makita, M., & Shibasaki, K. 1985, in Theoretical Problems in High Resolution Solar Physics, ed. H. U. Schmidt (Garching: MPA), 313
 Scannapieco, E. S., & Ferreira, P. G. 1997, *PhRvD*, 56, R7493
 Scóccola, C., Harari, D., & Mollerach, S. 2004, *PhRvD*, 70, 063003
 Seehafer, N. 1990, *SoPh*, 125, 219
 Seljak, U., & Zaldarriaga, M. 1997, *PhRvL*, 78, 2054
 Singh, N. K., Käpylä, M. J., Brandenburg, A., et al. 2018, *ApJ*, 863, 182
 Sokoloff, D. D., Bykov, A. A., Shukurov, A., et al. 1998, *MNRAS*, 299, 189
 Volegová, A. A., & Stepanov, R. A. 2010, *JETP*, 90, 637
 Warnecke, J., Brandenburg, A., & Mitra, D. 2011, *A&A*, 534, A11
 Warnecke, J., Brandenburg, A., & Mitra, D. 2012, *JSWSC*, 2, A11
 Zaldarriaga, M., & Seljak, U. 1997, *PhRvD*, 55, 1830
 Zhang, H., Sakurai, T., Pevtsov, A., et al. 2010, *MNRAS*, 402, L30